Molecular Systems Design & Engineering

PAPER

View Article Online
View Journal | View Issue

Cite this: *Mol. Syst. Des. Eng.*, 2018, 3, 275

Unusual solvent polarity dependent excitation relaxation dynamics of a bis[*p*-ethynyldithiobenzoato]Pd-linked bis[(porphinato)zinc] complex†

Jaehong Park, *[abc] Tae-Hong Park,[bd] Louise E. Sinks,[b] Pravas Deria, [be] Jiyong Park, [f] Mu-Hyun Baik [f] and Michael J. Therien *[c]

Received 1st January 2018,
Accepted 29th January 2018

DOI: 10.1039/c8me00001h

rsc.li/molecular-engineering

We report the synthesis and excited-state dynamics of a bis[*p*-ethynyldithiobenzoato]Pd(II)-bridged bis[(porphinato) zinc(II)] complex (**PZn–Pd(edtb)$_2$–PZn**) that exhibits unusual solvent dielectric (ε)-dependent excited-state relaxation behavior. In nonpolar toluene solvent, **PZn–Pd(edtb)$_2$–PZn** manifests an ultrafast $S_1 \rightarrow T_1$ intersystem crossing time constant ($\tau_{ISC} \approx 2$ ps), a broad, high-oscillator strength $T_1 \rightarrow T_n$ transient absorption manifold ($\lambda_{max}(T_1 \rightarrow T_n) = 940$ nm), and a near unity triplet-state formation quantum yield ($\Phi_T \approx 1$; $\tau_T = 2.2$ μs). In contrast, in moderately polar solvents (*e.g.*, dichloromethane (DCM) or THF), the $S_1 \rightarrow T_1$ intersystem crossing quantum yield is significantly suppressed ($\Phi_T \approx 0.2$; $\tau_F \approx 60$ ps in DCM). Comparative femtosecond transient absorption studies in DCM and mixed DCM/toluene solvent systems reveal a new low-energy stimulated emission signal, the λ_{em}^{max} of which is highly sensitive to solvent polarity. The lack of spectral signatures for radical species, and the emergence of intense stimulated emission indicate an additional low energy electronically excited-state (S*), populated *via* S_1-state relaxation, that also possesses substantial singlet character. As solvent polarity is progressively increased, the energy of S* progressively decreases, eventually becoming lower than the S_1 state and providing an excited-state relaxation channel that bypasses T_1 state formation. These data show that the nature of the **PZn–Pd(edtb)$_2$–PZn** excited-state dynamics is strongly influenced by the solvent dielectric, and that this Pd(II)-based linker motif offers new opportunities to engineer excited-state spin distributions and lifetimes in strongly conjugated chromophore assemblies.

Design, System, Application

Transition metals define molecular design tools to modulate chromophore optical, electronic, electrochemical, and magnetic properties in conjugated organic frameworks. Palladium-containing ligand frameworks that can form square or rectangular planar structures define a strategy to augment the electronic coupling between transition metals and π-conjugation organic system; in general, however, Pd-containing bridges do not guarantee significant electronic coupling between the metal ions and the organic π-conjugative systems. A model compound (PZn–Pd(edtb)$_2$–PZn), composed of a bis[*p*-ethynyldithiobenzoato]Pd(II) linker (Pd(edtb)$_2$) and zinc porphyrin (PZn) monomers was synthesized; spectroscopic studies of this complex revealed that the **PZn–Pd(edtb)$_2$–PZn** design thus successfully couples a **Pd(edtb)$_2$** core and *meso*-ethynylated **PZn** chromophores to realize a π-conjugated supermolecule in which Pd(II) d orbitals participate in electronic coupling over a large porphyrin center-to-center distance (~29.4 Å). This work demonstrates that the Pd(edtb)$_2$ bridge is an effective transition metal-containing motif: i) to modulate the photophysics of porphyrin arrays, ii) to enhance the intersystem crossing rate constant, and iii) to introduce functionality that tunes the triplet-state formation quantum yield as a function of solvent polarity without modifying porphyrin structure.

[a] *Department of Molecular Engineering, Graduate School of Engineering, Kyoto University, Nishikyo-ku, Kyoto, 615-8510, Japan. E-mail: j.park@moleng.kyoto-u.ac.jp*
[b] *Department of Chemistry, University of Pennsylvania, 231 South 34th Street, Philadelphia, Pennsylvania 19104-6323, USA*
[c] *Department of Chemistry, Duke University, French Family Science Center, 124 Science Drive, Durham, North Carolina 27708-0346, USA. E-mail: michael.therien@duke.edu*
[d] *Nuclear Chemistry Research Division, Korea Atomic Energy Research Institute, Daejeon, 34057, South Korea*
[e] *Department of Chemistry, Southern Illinois University, 1245 Lincoln Drive, Carbondale, Illinois 62901, USA*
[f] *Department of Chemistry, Korea Advanced Institute of Science and Technology (KAIST) & Center for Catalytic Hydrocarbon Functionalizations, Institute for Basic Science (IBS), Daejeon 34141, South Korea*

† Electronic supplementary information (ESI) available: Details of materials, synthetic procedures, characterization data, spectroscopic data acquisition and analysis, additional optical and transient dynamical data, electronic structure computational data. See DOI: 10.1039/c8me00001h

Introduction

Given their unique optical, electronic, electrochemical, excited-state properties, a great deal of research effort has been devoted to the molecular engineering of porphyrin arrays. The most compelling of these arrays feature molecular bridges that give rise to substantial electronic coupling between the porphyrin units, driving optical, electronic, electrochemical, and magnetic properties having utility in applications that span photovoltaics,[1,2] nonlinear optics,[3–7] molecular electronics,[8–11] biological imaging,[12,13] and photodynamic therapy.[14,15] In the molecular design of such porphyrin arrays, earlier work highlights the importance of the bridging units in the modulation of key properties of these supermolecular systems.[16,17]

Multiple organic conjugative motifs have been employed in porphyrin array design, and the photophysics of these systems have been established.[16–26] On the other hand, porphyrins that take advantage of transition metal-containing bridging moieties represent an area of growing interest, as these motifs can play profound roles in modulating excited-dynamics, spintronic functionality, and charge transport. For example, porphyrin arrays linked by metal-containing bridges can facilitate enhanced triplet-state formation quantum yields, and augmented charge transfer interactions in these supermolecules.[27–39] Such intimate connections between heavy metal centers and organic frameworks inspire new designs for engineering materials for optical, electronic and spintronic applications.[4,40–50]

In particular, palladium- or platinum-containing ligand frameworks that can form square or rectangular planar structures define an interesting strategy to electronically couple porphyrin planes *via* building blocks that enable electronic communication that involves d orbitals.[27,30,31,34–36,38,39] In general, porphyrin arrays consisting of Pd-/Pt-containing bridges do not guarantee significant electronic coupling between the metal ions and the porphyrin π-ligand framework. Fundamental structure–property relationships for such supermolecular chromophores that manifest strong electronic coupling between the porphyrin units and metal-containing bridges are under-developed, and thus motivate the studies described below.

Here, we report the synthesis and excited-state dynamics of a bis[*p*-ethynyldithiobenzoato]Pd(II)-bridged bis-[(porphinato)zinc] complex (**PZn–Pd(edtb)$_2$–PZn**; Scheme 1). **PZn–Pd(edtb)$_2$–PZn** consists of two (porphinato)zinc(II) (**PZn**) units and a bis[*p*-ethynyldithiobenzoato]palladium(II) (**Pd(edtb)$_2$**) bridge that covalently connects the **PZn** moieties *via* the macrocycle *meso*-positions. This **PZn–Pd(edtb)$_2$–PZn** design takes advantage of a **Pd(dtb)$_2$** core that provides substantial conjugation between the phenyl and CS_2 entities.[51,52] Previous optical and computational studies highlight the enhanced conjugative interactions between the terminal phenyl units made possible by the square planar palladium(II) coordination environment.[53] Porphyrin arrays with bridging motifs involving ethynes, and related conjugative spacers such as 1,3-butadiyne, 4,7-diethynylbenzo[*c*][1,2,5]thiadiazole and 4,8-diethynylbenzo[1,2-*c*:4,5-*c*′]bis([1,2,5]thiadiazole) that take advantage of linkage connectivity involving the porphyrin *meso*-positions, display augmented ground- and excited-state electronic interactions.[23] This enhanced electronic communication between the antipodal porphyrin units derives in part from a modest degree of quinoidal character made possible by the ethynyl connectivity (Scheme 1).[16–18,20,23] The **PZn–Pd(edtb)$_2$–PZn** design thus couples a **Pd(dtb)$_2$** core and *meso*-ethynylated **PZn** chromophores to realize a π-conjugated supermolecule in which Pd(II) d orbitals participate in electronic coupling over a large porphyrin center-to-center distance (~29.4 Å). The **PZn–Pd(edtb)$_2$–PZn** electronic absorption spectrum (Fig. 1) demonstrates transition manifolds that derive from extensive mixing of the porphyrin B- (Soret) ($S_0 \rightarrow S_2$) and Q-band ($S_0 \rightarrow S_1$) transitions.[16,18,23,54–58] Pump–probe transient absorption (TA) spectroscopy of **PZn–Pd(edtb)$_2$–PZn** in nonpolar toluene (Tol) solvent shows: i) a near-unity triplet-state formation quantum yield (Φ_T) and a 2.0 ps of $S_1 \rightarrow T_1$ intersystem crossing time constant (τ_{ISC}), and ii) a $T_1 \rightarrow T_n$ induced absorption (IA) band ($\lambda_{max}(T_1 \rightarrow T_n)$ = 940 nm) in the NIR spectral domain that is absent for the (porphinato)Zn(II) and **Ph–Pd(edtb)$_2$–Ph** building block

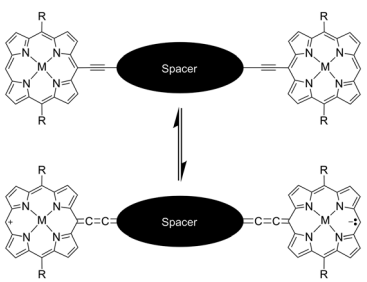

Scheme 1 Conjugated porphyrin arrays and quinoidal resonance contribution made possible by the macrocycle *meso*-ethynyl connectivity.

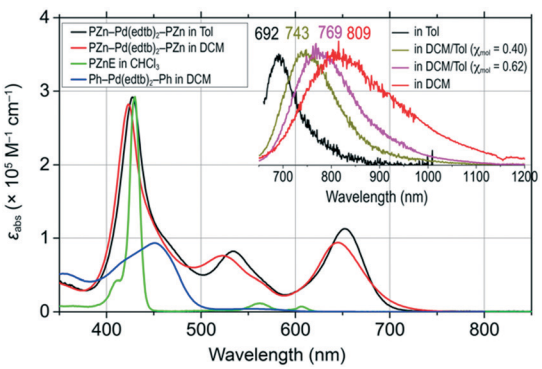

Fig. 1 Comparative electronic absorption spectra of **PZn–Pd(edtb)$_2$–PZn** in toluene (Tol; black) and CH_2Cl_2 (DCM; red) solvents, relative to **PZnE** (green), and **Ph–Pd(edtb)$_2$–Ph** (blue) benchmarks. Inset shows normalized corrected room-temperature emission spectra of **PZn–Pd(edtb)$_2$–PZn** [black: toluene; brown: DCM/Tol (χ_{mol} = 0.40); purple: DCM/Tol (χ_{mol} = 0.62); red: DCM]. χ_{mol} corresponds to the DCM mole fraction = (mole of DCM)/(total moles of solvent). Experimental conditions: λ_{ex} = 652 nm for toluene; λ_{ex} = 640 nm for DCM/Tol (χ_{mol} = 0.40), DCM/Tol (χ_{mol} = 0.62), and DCM solvents.

chromophores (Scheme 1). While ^{3}[PZn–Pd(edtb)$_2$–PZn]* features a T_1-state lifetime (τ_T) of 2.2 μs in toluene solvent, excited-state dynamical data acquired in moderately polar solvents such as dichloromethane (DCM) and tetrahydrofuran (THF) demonstrate dramatically reduced excited-state lifetimes, with an extensive fraction of the excited state population (~80–85%) exhibiting picosecond timescale relaxation dynamics, giving rise to Φ_T values ≈ 0.2. The lack of spectral signatures indicative of radical species, and the emergence of intense stimulated emission in these transient spectral data, indicate a low energy electronically excited-state (S*) that possesses substantial singlet character. The extraordinary sensitivity of the energy of this new electronically excited-state that possesses substantial singlet character (S*) to the nature of the solvent dielectric relative to that exhibited by the T_1 state suggests that bis[*p*-ethynyldithiobenzoato]Pd(II) and related conjugated bridges offer new opportunities to engineer excited-state spin distributions and lifetimes.

Results and discussion

Scheme 2 outlines the synthesis of bis[4-[(10′,20′-bis(2′,6′-bis(3,3-dimethyl-1-butyloxy)phenyl)porphinato)zinc(II)ethyn-5′-yl]dithiobenzoato]palladium(II) (**PZn–Pd(edtb)$_2$–PZn**); detailed synthetic procedures and characterization data are described in the ESI.† The deprotection of precursor (**3**)[59] and subsequent metalation with $PdCl_2$ induced precipitation of a dark solid; filtration followed by acetone/MeOH washing afforded analytically pure **PZn–Pd(edtb)$_2$–PZn**.

Comparative solvent-dependent electronic absorption spectra of **PZn–Pd(edtb)$_2$–PZn** are displayed in Fig. 1 and S2,† along with those for the 5-ethynyl(porphinato)zinc(II) (**PZnE**) and bis[4-[(3′,5′-di-*t*-butylphenyl)ethynyl]dithiobenzoato]-palladium(II) (**Ph–Pd(edtb)$_2$–Ph**) reference compounds; the corresponding electronic absorption spectroscopic data are tabulated in Table 1 and S1.† The absorption spectral features of **PZn–Pd(edtb)$_2$–PZn** differ markedly from those of the reference compounds (**PZnE** (ref. 60) and **Ph–Pd(edtb)$_2$–Ph** (ref. 61)). Electronic absorption spectra of **PZn–Pd(edtb)$_2$–PZn** display a new, low energy electronic transition manifold that features a substantial extinction coefficient (ε_{abs} = ~10^5 M^{-1} cm^{-1} near 650 nm), contrasting those of **PZnE** or **Ph–Pd(edtb)$_2$–Ph**.[53,61] This absorption band centered at 650 nm resembles those of highly conjugated bis[(porphinato)metal] complexes, and derives from symmetry breaking of the porphyrin structural units, and oscillator strength redistributions that stem from conjugation expansion.[16,18,23,54–58] DFT computational studies that explore dihedral angle-dependent conformational energies between hypothetical planar 5-ethynylporphyrin and bis(dithiobenzoato)Pd(II) units, or between related 5-phenylethynylporphyrin and the bis(dithioate)-Pd(II) moieties (Fig. S3†) for a DFT-optimized **PZn–Pd(edtb)$_2$–PZn** structure, suggest a substantial population of conformers having modest porphyrin-bridge-porphyrin interplanar torsional angles at ambient temperature.

Table 1 Spectroscopic data acquired for **PZn–Pd(edtb)$_2$–PZn** in toluene, CH_2Cl_2, and THF solvents

	PZn–Pd(edtb)$_2$–PZn		
Solvent	Toluene	CH_2Cl_2	THF
λ_{abs} ($S_0 \rightarrow S_1$) [nm]	652	645	687
λ_{em}[a] [nm]	692 (1656)	809 (3205)	869 (2581)
Stokes shift[b] [cm^{-1}]	887	3143	3049
τ_F[c] [ps]	<15[f]	60	141
(Φ_F, %)	(<0.1)	(0.5)	(1.3)
τ_{es}[d] [ps]	2.0	54	144
τ_T [μs]	2.2	2.9	—
(Φ_T, %)[e]	(~100)	(~20)	(~15)

[a] Numbers in parentheses correspond to spectral breadths (FWHM) of the respective transitions in units of cm^{-1}. [b] The Stokes shift was taken as the energy difference between the λ_{em}^{max} and λ_{em}^{max} values. [c] Fluorescence lifetimes were determined from time-resolved emission experiments. [d] Excited singlet-state lifetimes derive from femtosecond transient absorption experiments. [e] The quantum yield of triplet formation (Φ_T) was calculated from femtosecond transient experimental data (see ESI for details). [f] The time-resolved fluorescence signals of **PZn–Pd(edtb)$_2$–PZn** in toluene decays within our instrumental temporal resolution of ~15 ps. Therefore, the τ_F should be less than 15 ps.

Room-temperature steady-state emission spectra of **PZn–Pd(edtb)$_2$–PZn** in various solvent systems are shown in Fig. 1 (inset); corresponding spectroscopic data are compiled in Table 1. **PZn–Pd(edtb)$_2$–PZn** in toluene shows an emission band with a λ_{em}^{max} at 692 nm. Note that **PZnE** displays two emission peaks at 607 and 662 nm that mirror its Q-band absorption spectrum; notably these fluorescence bands feature no solvent polarity dependence.[60] **Ph–Pd(edtb)$_2$–Ph** does not emit at room temperature. These emission data for **PZnE** and **Ph–Pd(edtb)$_2$–Ph** indicate that PZn units and the bis[*p*-ethynyldithiobenzoato]Pd(II) bridge are strongly coupled in **PZn–Pd(edtb)$_2$–PZn**. The Fig. 1 (inset) solvent-dependent emission spectra for **PZn–Pd(edtb)$_2$–PZn** are characterized by broad emission bands (full-width-at-half-maximum (FWHM) = 1656 to 3205 cm^{-1}), the λ_{em}^{max} values of which vary from ~690 to ~810 nm [λ_{em}^{max} = 692 nm, toluene (ε = 2.38); λ_{em}^{max} = 809 nm, DCM (ε = 9.1)],[62] stand in sharp contrast to

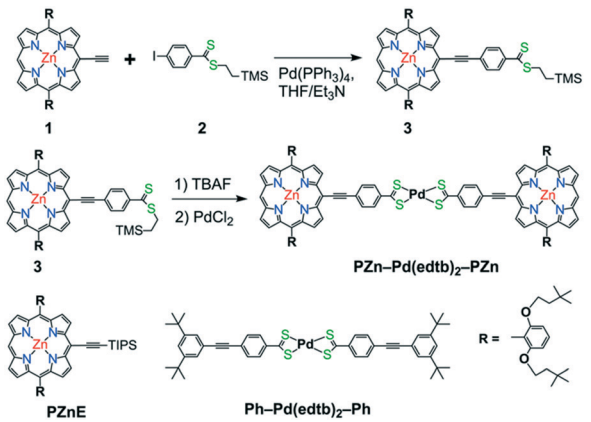

Scheme 2 Synthesis of **PZn–Pd(edtb)$_2$–PZn** and molecular structures of **PZnE**, and **Ph–Pd(edtb)$_2$–Ph**.

corresponding electronic absorption spectra which vary little as a function of solvent. These **PZn–Pd(edtb)$_2$–PZn** emission spectra highlight: i) a broader FWHM of the DCM emission band (3205 cm^{-1}) relative to toluene (1656 cm^{-1}), ii) a DCM Stokes shift (3143 cm^{-1}) that is more than three-fold larger than that in toluene (887 cm^{-1}), and iii) a fluorescence quantum yield (Φ_F) that is substantially larger in DCM (Φ_F ~0.5%) relative to toluene solvent (Φ_F < 0.1%). These marked disparate absorption and emission spectral characteristics suggest that the ground state is largely non-polar, while the emissive excited-state is dipolar in character. Time-resolved fluorescence spectroscopic measurements determine respective **PZn–Pd(edtb)$_2$–PZn** fluorescence lifetimes (τ_F values) of 60 ps and <15 ps (unresolved) in DCM and toluene solvents (Table 1, Fig. S4†). Note that the magnitude of the τ_F value determined for **PZn–Pd(edtb)$_2$–PZn** in toluene corresponds to a timescale similar to the instrumental temporal resolution limit (~15 ps), and therefore the τ_F cannot be accurately determined and its upper limit is 15 ps. The τ_F less than 15 ps for **PZn–Pd(edtb)$_2$–PZn** in toluene is consistent with the low Φ_F value (<0.1%) in this medium.

The excited-state dynamics of **PZn–Pd(edtb)$_2$–PZn** was further interrogated *via* femtosecond (fs) and nanosecond transient absorption (TA) spectroscopic experiments. Fig. 2a displays representative fs TA spectra of **PZn–Pd(edtb)$_2$–PZn** in toluene at selected time delays following photoexcitation (λ_{ex} = 650 nm). Conventional (porphinato)Zn(II) complexes are characterized by nanosecond (ns) timescale lowest singlet excited state (S_1-state) lifetimes, prominent induced absorption (IA) bands in the 400–650 nm spectral domain, and a broad low oscillator strength IA band in the 650–900 nm spectral region that is ascribed to an $S_1 \rightarrow S_n$ transition manifold.[63–65] On the other hand, the fs TA spectra acquired for **PZn–Pd(edtb)$_2$–PZn** in toluene (Fig. 2a) manifest the following features: i) ground state bleaching (GSB) bands at ~550 nm and ~650 nm, ii) an IA band, peaking at ~500 nm that is evident at t_{delay} ~1 ps and overlaps with the GSB bands at ~550 nm and ~650 nm, iii) an IA band peaking at ~510 nm that is evident at t_{delay} > ~50 ps, and iv) an intense IA band at the near-infrared (NIR) spectral domain (720–1200 nm, λ_{abs}^{max} ~940 nm) that grows in intensity over time delays spanning several tens of picoseconds, and persists beyond our instrumental delay limit (up to 3 ns). Note that the IA bands at ~510 nm overlap with IA bands evident at t_{delay} = 1 μs in the corresponding nanosecond-to-microsecond time domain TA spectroscopic experiments (Fig. S5a†). As the decay dynamics evident on this timescale are sensitive to molecular oxygen exposure, we attribute these IA bands to $T_1 \rightarrow T_n$ transitions of ^{3}[**PZn–Pd(edtb)$_2$–PZn**] ($\lambda_{max}(T_1 \rightarrow T_n)$ = 940 nm; *vide infra*). Over time delays that extend up through 3 ns, no GSB recovery was observed, indicating a near-unity quantum yield of $S_1 \rightarrow T_1$ intersystem crossing (Φ_T). Nanosecond (ns)-to-microsecond (μs) time domain TA spectroscopic data acquired in degassed toluene (Fig. S5a and b†) determine a T_1-state lifetime (τ_T) of 2.2 μs.

PZn–Pd(edtb)$_2$–PZn pump-probe transient absorptive dynamical data acquired in toluene solvent were analyzed using multiwavelength global fitting (Fig. S7†). The NIR IA signals

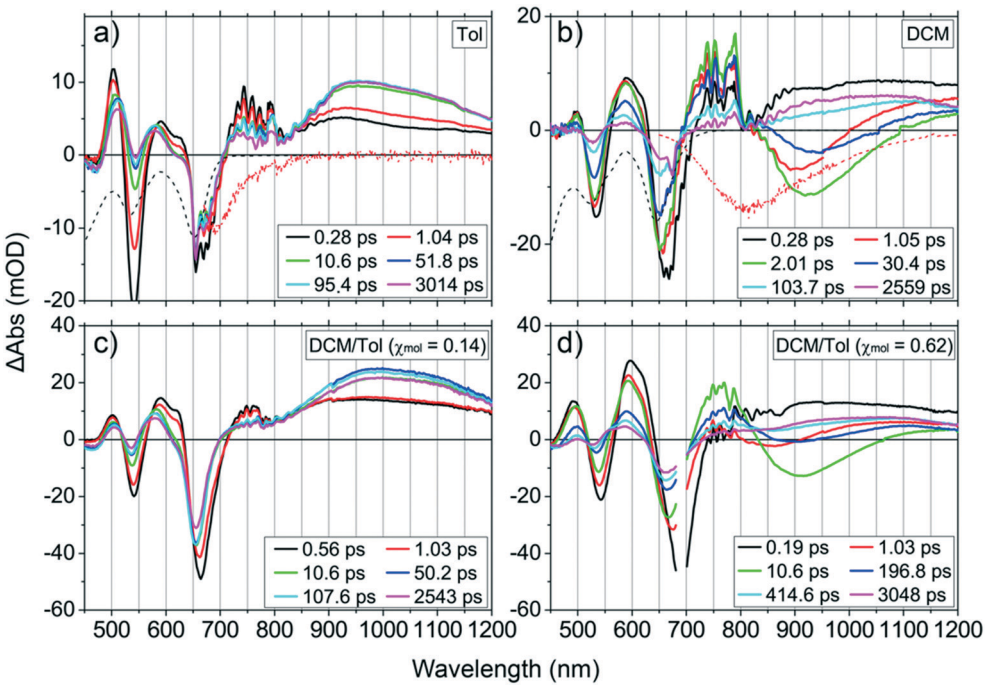

Fig. 2 Representative femtosecond transient absorption spectra acquired for **PZn–Pd(edtb)$_2$–PZn** in: (a) toluene, (b) DCM, (c) DCM/Tol (χ_{mol} = 0.14), and (d) DCM/Tol (χ_{mol} = 0.62), at time delays noted. Experimental conditions: λ_{ex} = 650, 671, 675, 690 nm for (a)–(d), respectively; pump energy = ~0.3 μJ per pulse; temperature = 20 °C. Inverted steady-state absorption (black dashed line) and emission spectra (red dotted line) are displayed for comparison.

characteristic of electronically excited ^{3}[**PZn–Pd(edtb)$_2$–PZn**] exhibit two rise time components of 2.0 ps and 16 ps, which are attributed to $S_1 \rightarrow T_1$ intersystem crossing and chromophore–chromophore torsional relaxation, respectively. The 2.0 ps time constant is associated with the decay of the $S_1 \rightarrow S_n$ IA signal at 743 nm in Fig. 2a and the stimulated emission (SE) signal evident at 677 nm, which probes the depletion dynamics of the S_1-state. Thus, we can assign the $S_1 \rightarrow T_1$ intersystem crossing time constant (τ_{ISC}) to be 2.0 ps. Note that the 16 ps time constant is associated with a substantial increase in the intensity of the $T_1 \rightarrow T_n$ NIR IA band; previous photophysical studies that interrogate ethyne-linked (porphinato)Zn(II)-based multichromophore systems indicate that this process is linked to structural equilibration governed by chromophore–chromophore torsional dynamics.[22,65–68] This spectral evolution probed in toluene underscores that the initially prepared **PZn–Pd(edtb)$_2$–PZn** excited state undergoes fast $S_1 \rightarrow T_1$ intersystem crossing (τ_{ISC} ~2.0 ps), congruent with the low Φ_F value (<0.1%) and the unresolved fluorescence lifetime within our temporal resolution ($\tau_F < 15$ ps) in this solvent; Fig. 4C data highlight these dynamics.

In earlier work, Duncan *et al.* reported palladium(II)-containing porphyrin arrays featuring a *meso*-to-*meso* ethyne-bridged linkage topology, showing that this design accelerates $S_1 \rightarrow T_1$ intersystem crossing (τ_{ISC} = 8.6 and 52.0 ps for Pd-porphyrin dimers and trimers relative to analogous arrays that featured a porphyrin central zinc ion.[55] These data acquired for **PZn–Pd(edtb)$_2$–PZn** suggest that the **Pd(edtb)$_2$** bridge provides an even more effective strategy to accelerate the $S_1 \rightarrow T_1$ intersystem crossing rate constant in these related supermolecules.

PZn–Pd(edtb)$_2$–PZn excited-state dynamics were further explored in moderately polar DCM solvent (Fig. 2b). The TA spectral data acquired in DCM at ~0.3 ps < t_{delay} < ~3 ns are clearly distinguished from those in toluene (Fig. 2a); note in this regard that the spectral evolution in DCM, occurring within the initial 3 ns following optical excitation is highly complicated, showing marked evolution of IA and SE signals.

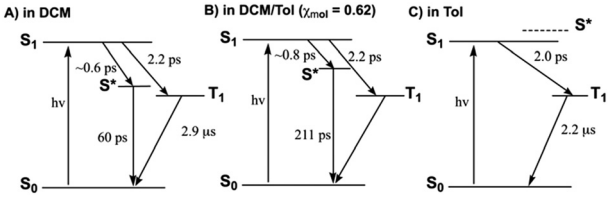

Fig. 4 Summary of the solvent polarity dependent excited state dynamics of **PZn–Pd(edtb)$_2$–PZn** in: (A) DCM, (B) a DCM/Tol mixture (χ_{mol} = 0.62), and (C) toluene.

To help clarify this complex TA spectral evolution, Fig. 3 highlights the excited-state dynamics that characterize four distinct time domains: a) 0.1 ps < t_{delay} < 0.4 ps, b) 0.4 ps < t_{delay} < 4 ps, c) 10 ps < t_{delay} < 100 ps, d) 100 ps < t_{delay} < 3 ns.

1. At t_{delay} < 0.4 ps (Fig. 3a): the TA spectra in this time domain are characterized by a broad IA band spanning the 720–1300 nm spectral regime; note that this IA spectral feature is identical to that manifest in toluene solvent over similar delay times (*e.g.*, t_{delay} < 1 ps, Fig. 2a) and is assigned to the $S_1 \rightarrow S_n$ transition. Also evident is a pronounced blue shift of the Q-state GSB signal (from 664 nm to 660 nm), along with an apparent intensity decrease at the earliest time delays: based on the corresponding position of the Q-state absorption maximum in the steady-state spectrum (645 nm), these spectral data indicate a significant contribution of S_1 state stimulated emission (SE1) over these time delays, congruent with the Fig. 2a steady state and transient dynamical

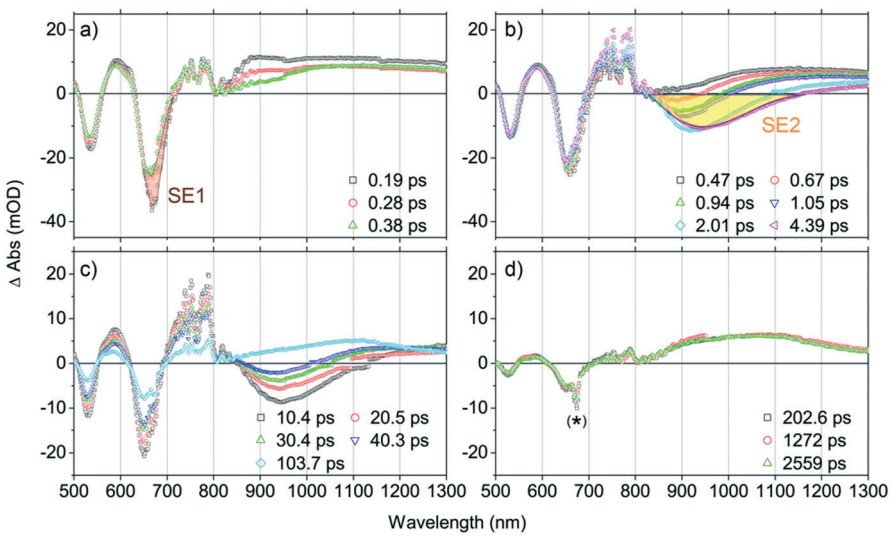

Fig. 3 Representative femtosecond transient absorption spectral evolution of **PZn–Pd(edtb)$_2$–PZn** in DCM solvent, recorded at the time delays noted: (a) t_{delay} = 0.1–0.4 ps, (b) 0.4–4 ps, (c) 10–100 ps, and (d) 200–2500 ps. Experimental conditions: λ_{ex} = 671 nm; pump energy = 300 nJ per pulse; magic angle polarization; ambient temperature. The artifact at ~671 nm (denoted with *) derives from scattering of the excitation beam. The spectral signatures corresponding to SE1 and SE2 are highlighted in brown and yellow, respectively, in panels a) and b).

data acquired in toluene at early time delays (*e.g.*, ~665 nm at $t_{delay} < 1$ ps).

2. At 0.4 ps $< t_{delay} <$ 4 ps (Fig. 3b): these TA spectra exhibit: i) a broad negative spectral feature (800–1100 nm), that displays a dynamic red-shift through time delays up to ~4 ps; ii) an abrupt decrease of the SE1 contribution at ~660 nm, suggesting the depletion of the initially prepared S_1-state population; and iii) a conspicuous lack of GSB recovery over this time domain, indicating migration of the S_1-state population into another excited-state. Given the steady-state emission spectrum of **PZn–Pd(edtb)$_2$–PZn** in DCM (Fig. 1) and the corresponding Q-state absorption band position (645 nm), we attribute this broad negative spectral feature (800–1100 nm) to an additional SE signal (SE2) characteristic of an excited-state (S*) that is significantly lower in energy than the initially prepared S_1-state. Note that the ground-state electronic absorption spectrum acquired in DCM solvent exhibits a low energy absorption manifold centered at 645 nm and that SE1 (~660 nm) shows a mirror-image relationship to this manifold. As no ground-state electronic absorption is observed over the 800–1100 nm spectral domain, the S* state must be accessible only from S_1, and not from a direct $S_0 \rightarrow S^*$ transition. In this regard, **PZn–Pd(edtb)$_2$–PZn** displays excited-state dynamics that resemble those of several push–pull polyenes and carotenoids such as peridinin: in polar solvents, these chromophores access an emissive excited nuclear conformation that does not resemble the ground state, and thereby manifest an additional SE band evident at a longer wavelength than that for $S_1 \rightarrow S_0$ emission. These chromophores, akin to **PZn–Pd(edtb)$_2$–PZn**, also display no direct $S_0 \rightarrow S^*$ electronic transition.[69–72] Note that this NIR SE2 is also observed in THF (Fig. S8†) but is absent in toluene (Fig. 2a), suggesting that production of S* depends on solvent polarity (*vide infra*).

3. At 10 ps $< t_{delay} <$ 100 ps (Fig. 3c): over this time domain, TA spectral evolution highlights the time-dependent diminution of the SE2 signal at ~950 nm along with the corresponding recovery of GSB bands at ~550 nm and ~650 nm. These data contrast those acquired in toluene, where no measurable excited-state relaxation is evident over the initial 3 ns following optical excitation (Fig. 2a). As $S^* \rightarrow S_0$ stimulated emission (SE2) diminishes at $t_{delay} >$ 100 ps in DCM, an IA band emerges over the NIR spectral domain.

4. At 100 ps $< t_{delay}$ (Fig. 3d): no TA spectral evolution is observed from 100 ps through the t_{delay} limit of the instrument (~3 ns); note that these TA spectra resemble those acquired at $t_{delay} >$ 10 ps in toluene solvent (Fig. 2a). This NIR spectral signature decays with a time constant (τ_T) of 2.9 μs, determined from ns-TA spectroscopy (Fig. S5c and d†) and is therefore assigned as a $T_1 \rightarrow T_n$ transition manifold. The Φ_T in DCM was determined to be ~0.2 from the methods described in the ESI.†

A multiwavelength global fit of the TA spectroscopic data acquired for **PZn–Pd(edtb)$_2$–PZn** in DCM solvent determines time constants for SE1 decay (τ_{S1} = 0.44 ps), SE2 decay (τ_{S^*} = 54 ps), and GSB recovery (τ_{GSB} = 61 ps). Note that the 54 ps SE2 decay time constant is consistent with τ_{GSB}, as well as the **PZn–Pd(edtb)$_2$–PZn** emission lifetime (τ_F = 60 ps; Fig. S4†). Therefore, the $S^* \rightarrow S_0$ relaxation rate corresponds to (54 ps)$^{-1}$.

With respect to the mechanism of S_1 state depletion and T_1 state formation, two possibilities can be considered: i) sequential population transfer from S* to T_1 ($S_1 \rightarrow S^* \rightarrow T_1$), or ii) parallel processes that allow for both $S_1 \rightarrow T_1$ intersystem crossing and $S_1 \rightarrow S^*$. The combination of the T_1-state formation quantum yield (Φ_T ~0.2) in DCM, the lifetimes of the S_1 and S* states (τ_{S1} = 0.44 ps; τ_{S^*} = 54 ps), and the absence of a slow rise of the $T_1 \rightarrow T_n$ transition beyond $t_{delays} >$ 200 ps (Fig. 3d) strongly indicate that the T_1-state population derives from $S_1 \rightarrow T_1$ intersystem crossing that competes with $S_1 \rightarrow S^*$ relaxation.‡ The $S_1 \rightarrow T_1$ intersystem crossing time constant (τ_{ISC}) is therefore determined to be 2.2 ps (eqn (1) and (2)):

$$\Phi_T = \frac{k_{ISC}}{k_{NR} + k_R + k_{S1\rightarrow S^*} + k_{ISC}} = 0.2 \quad (1)$$

$$\tau_{S1} = \frac{1}{k_{NR} + k_R + k_{S1\rightarrow S^*} + k_{ISC}} = 0.44\ \text{ps} \quad (2)$$

where k_{NR}, k_R, $k_{S1\rightarrow S^*}$, k_{ISC} are the respective decay rates of the S_1 state through nonradiative relaxation (NR), radiative relaxation (R), $S_1 \rightarrow S^*$ relaxation, and $S_1 \rightarrow T_1$ intersystem crossing processes. Note that the magnitude of τ_{ISC} determined in DCM (2.2 ps) matches that measured in toluene (τ_{ISC} = 2.0 ps; Fig. 2a), suggesting that the **PZn–Pd(edtb)$_2$–PZn** $S_1 \rightarrow T_1$ intersystem crossing rate constant varies little with solvent polarity.

What clearly differs as a function of solvent polarity is the S*-state accessibility from S_1. Because GSB recovery is negligible in DCM at $t_{delays} <$ ~10 ps, $\tau_{S1\rightarrow S^*}$ can be determined to be ~0.6 ps, as the magnitudes of k_{NR} and k_R are significantly smaller than those for both $k_{S1\rightarrow S^*}$ and k_{ISC}. This 0.6 ps time constant for $S_1 \rightarrow S^*$ relaxation agrees with the emergence of the SE2 signal on the sub-picosecond timescale, shown in Fig. 3b. **PZn–Pd(edtb)$_2$–PZn** excited-state relaxation in DCM thus occurs predominantly through dynamical channels defined by $S_1 \rightarrow S^*$ and $S^* \rightarrow S_0$, with only a fraction (~0.2) of the initially prepared excited state returning to ground *via* the $S_1 \rightarrow T_1$ and $T_1 \rightarrow S_0$ pathway (Fig. 4A). The fast $S_1 \rightarrow T_1$ intersystem crossing time constant (~2 ps), and the even faster time constant for $S_1 \rightarrow S^*$ dynamics (~0.6 ps)

‡ If the $S^* \rightarrow T_1$ process is responsible for T_1-state formation, its $S^* \rightarrow T_1$ time constant $\left(\tau'_{ISC}\right)$ is determined to be ~300 ps, from the following equations: $\Phi'_T = \left(k'_{ISC}\right) / \left(k'_{NR} + k'_R + k'_{ISC}\right)$ and $\tau_{S^*} = 1 / \left(k'_{NR} + k'_R + k'_{ISC}\right)$, where Φ'_T is the quantum yield of triplet formation from $S^* \rightarrow T_1$, and k'_{NR}, k'_R, and k'_{ISC} are the decay rates of S*-state through nonradiative relaxation (NR), radiative relaxation (R) and $S^* \rightarrow T_1$ intersystem crossing processes, respectively.

determined for **PZn–Pd(edtb)$_2$–PZn** in DCM solvent suggests little or no contribution of structural dynamics of this large supermolecular system playing a role in these dynamics, as previous studies of porphyrin dimers featuring ethyne and butadiyne bridges have shown that the singlet-state structural relaxation time constants range between 10–30 ps.[22,65,73] In this regard, the solvent nature thus likely plays a crucial role in modulating excited state dynamics.

PZn–Pd(edtb)$_2$–PZn excited-state dynamics determined in DCM/toluene solvent mixtures provide insights into how relative S_1 and S* state energies vary as a function of solvent polarity. Fig. 1b, 2c and d, and S9† show steady-state emission and fs-TA spectra of **PZn–Pd(edtb)$_2$–PZn** recorded in solvents composed of various DCM : Tol molar ratios; in these solvents, DCM/Tol (χ_{mol}) represents the DCM mole fraction, the moles of DCM/(total moles of DCM and toluene in a mixture). In Fig. 2c, the **PZn–Pd(edtb)$_2$–PZn** TA spectra recorded in DCM/Tol (χ_{mol} = 0.14) resemble those acquired in neat toluene, and lack the SE2 signature. In contrast, the **PZn–Pd(edtb)$_2$–PZn** TA spectral evolution in DCM/Tol (χ_{mol} = 0.62) resembles that determined in neat DCM (Fig. 2d). Note, however, that in the DCM/Tol (χ_{mol} = 0.62) mixture, the SE2 signal emerges at ~900 nm, blue-shifted with respect to that observed in neat DCM (~950 nm, in Fig. 2b). Additional experiments further confirm that the SE2 peak position is clearly solvent-dependent: for example, in DCM/Tol (χ_{mol} = 0.40; Fig. S9†) the SE2 signal appears at ~850 nm.

This increasing blue shift of the SE2 signal with decreasing solvent polarity agrees with steady-state emission spectra highlighted in Fig. 1 (inset). The different positions of the steady-state emission spectra λ_{em}^{max} values and the SE2 signature stem from both a dynamic Stokes-shift contribution to SE2, and the overlap of SE2 and IA signals in the TA spectra (Fig. 3). As a result, in non-polar solvents such as toluene and DCM/Tol (χ_{mol} = 0.14), $S_1 \rightarrow S_0$ radiative relaxation is responsible for the steady-state emission highlighted in the Fig. 1 inset, whereas in moderately polar solvents (DCM, DCM/Tol (χ_{mol} = 0.40 and 0.62), or THF), the emission originates from the $S^* \rightarrow S_0$ radiative relaxation. Approximation of the dielectric constant (ε) of the DCM/Tol mixtures§ allows the emission peak energy ($\tilde{\nu}_{em}$) to be displayed as a function of the Onsager function ($f(\varepsilon) = 2(\varepsilon - 1)/(2\varepsilon + 1)$; Fig. S10†). These data (χ_{mol} = 0.40, 0.62, 1.0) highlight a linear increase of $\tilde{\nu}_{em}$ with decreasing $f(\varepsilon)$. Note, however, that $\tilde{\nu}_{em}$ for χ_{mol} = 0.0 (neat toluene) deviates from the linear fit line (red solid line in Fig. S10†): this dependence derives from the fact that in moderately polar solvent two different **PZn–Pd(edtb)$_2$–PZn** emitting states are manifest (S_1 and S*), while in neat toluene, only emission from S_1 is detected. From the linear fit line, the S* state in neat toluene is estimated to lie ~15 900 cm^{-1} above the ground state and higher in energy than S_1. For χ_{mol} = 0.14, where **PZn–Pd(edtb)$_2$–PZn** excited-state dynamical data (Fig. 2c) show no evidence for SE2, this analysis determines an S* state energy of ~14 700 cm^{-1}, which is also higher than the $\tilde{\nu}_{em}$ in toluene ($\tilde{\nu}_{em}$ = 14 400 cm^{-1}) and congruent with the near-unit Φ_T and similarity of the excited-state dynamics evinced in DCM/Tol (χ_{mol} = 0.14) and neat toluene solvent systems.

A multiexponential global fit for **PZn–Pd(edtb)$_2$–PZn** in DCM/Tol (χ_{mol} = 0.62) yields time constants of 0.6 ps, 3 ps, 211 ps, and a long component (>3 ns). The 0.6 ps component, related to the decay of SE1, corresponds to τ_{S1}. In both toluene and DCM, τ_{ISC} is ~2 ps; as τ_{ISC} shows little solvent dependence, Φ_T can be determined to be ~0.27 in DCM/Tol (χ_{mol} = 0.62). This Φ_T value determined from eqn (1) and (2) agrees with that evaluated from the TA spectral data (Φ_T = ~0.3), as described in the ESI.† From the Φ_T, τ_{S1}, and τ_{ISC} values, we determine $\tau_{S1 \rightarrow S^*}$ to be ~0.8 ps. **PZn–Pd(edtb)$_2$–PZn** excited-state dynamics determined in DCM/Tol (χ_{mol} = 0.62) are summarized in Fig. 4B.

Fig. 4 highlights the fact that the S* energy level is sensitive to small changes of solvent polarity, suggesting that this state may possess charge-transfer character; certainly, as S* may be destabilized relative to both S_1 and T_1, its electronic structure must diverge from both the initially prepared singlet and relaxed triplet states. Previously, the excited-state dynamics of other highly conjugated organic chromophoric systems such as peridinin[69–71] and push–pull type polyenes[72] have shown closely related solvent-polarity-dependent excited-state dynamical behaviors. TA spectroscopic studies of peridinin, for example, revealed two singlet excited states, one of which corresponded to a highly delocalized intramolecular charge transfer (ICT) state, which gives rise to sub-optical band gap stimulated emission only in polar solvents and no spectral signatures consistent with cation or anion radical species.[70] While the exact nature of the **PZn–Pd(edtb)$_2$–PZn** S* state manifest in polar solvents is obscure, congruent with the transient spectral signatures that characterize peridinin[69–71] and push–pull type polyenes,[72] these **PZn–Pd(edtb)$_2$–PZn** excited-state dynamical studies evince no spectroscopic hallmarks congruent with the light-driven formation of cation or anion radical species in polar solvents.[74]

Experimental

Materials and methods

All manipulations were carried out under Ar unless otherwise stated. CH_2Cl_2 and tetrahydrofuran (THF) were distilled over CaH_2 and Na/benzophenone under N_2, respectively. Triethylamine (Et_3N) was distilled over KOH under N_2. All NMR solvents were used as received. $Pd(PPh_3)_4$ was purchased from Strem Chemicals and used as received. Tetrabutylammonium fluoride (TBAF) (1 M THF solution, Aldrich) was further diluted to 0.1 M. For optical spectroscopy, HPLC grade toluene, CH_2Cl_2, and THF were purchased from Sigma Aldrich and purified by passing through alumina columns in a Puresolv solvent purification system (Innovative Technology, Inc., Amesbury, MA) before use. ACS spectrophotometric grade $CHCl_3$ was purchased from Sigma Aldrich and used as

§ Since the ε values of DCM/Tol mixtures are not available, these values were calculated from $\varepsilon(\chi_{mol}) = \chi_{mol}\varepsilon(\text{DCM}) + (1 - \chi_{mol})\varepsilon(\text{Tol})$.[77]

received. Synthetic details and characterization data are described in the ESI.†

Instrumentation

Electronic absorption spectra were collected using a Shimadzu UV-1700 UV-vis spectrophotometer or a Varian Cary-5000 UV-vis-NIR spectrophotometer. Steady-state emission spectra were obtained on FLS920P spectrophotometer (Edinburgh Instruments Ltd. Livingston, UK) in 1 cm quartz optical cells. A set of appropriate long-pass filters were used to remove second order scattering light from the lamp and grating for the excitation beam and to eliminate scattered excitation light on the emission collection pathway. Steady-state emission spectra were corrected using the correction factor generated by the manufacturer. Details of material characterization and time-resolved photoluminescence spectroscopy and femtosecond and nanosecond-microsecond transient absorption apparatus[75,76] are described in the ESI.†

Conclusion

In summary, we describe the synthesis of a bis[*p*-ethynyldithiobenzoato]Pd(II)-bridged bis[(porphinato)zinc(II)] complex (**PZn–Pd(edtb)$_2$–PZn**). Electronic absorption spectra of **PZn–Pd(edtb)$_2$–PZn** suggest extensive electronic delocalization in this supermolecule and highlight a new, low energy electronic transition manifold that features a substantial extinction coefficient (ε_{abs} = ~10^5 M^{-1} cm^{-1} near 650 nm), contrasting benchmark spectral data for simple (porphinato)zinc monomers and **Pd(edtb)$_2$**-bridged aryl units. Excited-state dynamical data acquired for **PZn–Pd(edtb)$_2$–PZn** demonstrate that this structure exhibits unusual solvent dielectric (ε)-dependent excited-state relaxation behavior. In nonpolar toluene solvent, **PZn–Pd(edtb)$_2$–PZn** manifests an ultrafast $S_1 \rightarrow T_1$ intersystem crossing time constant ($\tau_{ISC} \approx 2$ ps), a broad, high-oscillator strength $T_1 \rightarrow T_n$ transient absorption manifold in the NIR ($\lambda_{max}(T_1 \rightarrow T_n)$ = 940 nm), and a near unit triplet-state formation quantum yield ($\Phi_T \approx 1$; τ_T = 2.2 μs). The **Pd(edtb)$_2$** bridge thus demonstrates an effective motif to accelerate the $S_1 \rightarrow T_1$ intersystem crossing dynamics in organic molecular systems. In contrast, in moderately polar solvents (*e.g.*, CH_2Cl_2 (DCM) or THF), the $S_1 \rightarrow T_1$ intersystem crossing quantum yield is significantly suppressed ($\Phi_T \approx 0.2$; $\tau_F \approx 60$ ps in DCM) despite the similarly ultrafast τ_{ISC} (≈2.2 ps). Comparative femtosecond transient absorption studies in DCM and mixed DCM : Tol solvent systems reveal a new low-energy stimulated emission signal, the λ_{em}^{max} of which is highly sensitive to solvent polarity. The lack of spectral signatures for radical species and the emergence of intense stimulated emission indicate that this additional low-energy electronically excited-state (S*), populated *via* S_1-state relaxation, also possesses substantial singlet character. As solvent polarity is progressively increased from the toluene benchmark, transient dynamical data indicate that the energy of S* progressively decreases, eventually becoming lower than the S_1 state, providing an excited-state relaxation channel that bypasses T_1 state formation. These data show that the nature of the **PZn–Pd(edtb)$_2$–PZn** excited-state dynamics is strongly influenced by the solvent dielectric, and that this Pd(II)-based linker motif offers new opportunities to engineer excited-state spin distributions and lifetimes in strongly conjugated chromophore assemblies.

Conflicts of interest

There are no conflicts to declare.

Acknowledgements

This work was funded by the Division of Chemical Sciences, Geosciences, and Biosciences, Office of Basic Energy Sciences, of the U.S. Department of Energy through Grant DE-SC0001517. J. P. acknowledges The Kyoto University Research Fund for Young Scientists (Start-up) and JSPS KAKENHI Grant-in-Aid for Research Activity (Start-up Grant Number 17H06791). T.-H. P. acknowledges support from the National Research Foundation of Korea (2017M2A8A5014710). J.-Y. P. and M.-H. B. acknowledge support from the Institute for Basic Science (IBS-R10-D1) in Korea.

Notes and references

1 H.-P. Wu, Z.-W. Ou, T.-Y. Pan, C.-M. Lan, W.-K. Huang, H.-W. Lee, N. M. Reddy, C.-T. Chen, W.-S. Chao, C.-Y. Yeh and E. W.-G. Diau, *Energy Environ. Sci.*, 2012, **5**, 9843–9846.
2 L.-L. Li and E. W.-G. Diau, *Chem. Soc. Rev.*, 2013, **42**, 291–304.
3 T. Ishizuka, L. E. Sinks, K. Song, S.-T. Hung, A. Nayak, K. Clays and M. J. Therien, *J. Am. Chem. Soc.*, 2011, **133**, 2884–2896.
4 G.-J. Zhou and W.-Y. Wong, *Chem. Soc. Rev.*, 2011, **40**, 2541–2566.
5 M. de Torres, S. Semin, I. Razdolski, J. Xu, J. A. A. W. Elemans, T. Rasing, A. E. Rowan and R. J. M. Nolte, *Chem. Commun.*, 2015, **51**, 2855–2858.
6 S. U. Hassan, H. M. Asif, Y. Zhou, L. Zhang, N. Qu, J. Li and Z. Shi, *J. Phys. Chem. C*, 2016, **120**, 27587–27599.
7 N. Fukui, T. Kim, D. Kim and A. Osuka, *J. Am. Chem. Soc.*, 2017, **139**, 9075–9088.
8 G. Sedghi, L. J. Esdaile, H. L. Anderson, S. Martin, D. Bethell, S. J. Higgins and R. J. Nichols, *Adv. Mater.*, 2011, **24**, 653–657.
9 Z. Li, T.-H. Park, J. Rawson, M. J. Therien and E. Borguet, *Nano Lett.*, 2012, **12**, 2722–2727.
10 M. Noori, H. Sadeghi and C. J. Lambert, *Nanoscale*, 2017, **9**, 5299–5304.
11 M. D. Peeks, C. E. Tait, P. Neuhaus, G. M. Fischer, M. Hoffmann, R. Haver, A. Cnossen, J. R. Harmer, C. R. Timmel and H. L. Anderson, *J. Am. Chem. Soc.*, 2017, **139**, 10461–10471.
12 P. P. Ghoroghchian, P. R. Frail, K. Susumu, D. Blessington, A. K. Brannan, F. S. Bates, B. Chance, D. A. Hammer and M. J. Therien, *Proc. Natl. Acad. Sci. U. S. A.*, 2005, **102**, 2922–2927.

13 J. E. Raymond and T. Goodson III, *J. Phys. Chem. Lett.*, 2011, **2**, 329–333.
14 S. Achelle, P. Couleaud, P. Baldeck, M.-P. Teulade-Fichou and P. Maillard, *Eur. J. Org. Chem.*, 2011, **2011**, 1271–1279.
15 Z. Xiang, L. Zhu, L. Qi, L. Yan, Y. Xue, D. Wang, J.-F. Chen and L. Dai, *Chem. Mater.*, 2016, **28**, 8651–8658.
16 V. S.-Y. Lin, S. G. DiMagno and M. J. Therien, *Science*, 1994, **264**, 1105–1111.
17 T. Tanaka and A. Osuka, *Chem. Soc. Rev.*, 2015, **44**, 943–969.
18 V. S.-Y. Lin and M. J. Therien, *Chem. – Eur. J.*, 1995, **1**, 645–651.
19 P. J. Angiolillo, V. S.-Y. Lin, J. M. Vanderkooi and M. J. Therien, *J. Am. Chem. Soc.*, 1995, **117**, 12514–12527.
20 H. L. Anderson, *Chem. Commun.*, 1999, 2323–2330.
21 N. Aratani, A. Osuka, H. S. Cho and D. Kim, *J. Photochem. Photobiol., C*, 2002, **3**, 25–52.
22 I. V. Rubtsov, K. Susumu, G. I. Rubtsov and M. J. Therien, *J. Am. Chem. Soc.*, 2003, **125**, 2687–2696.
23 K. Susumu, T. V. Duncan and M. J. Therien, *J. Am. Chem. Soc.*, 2005, **127**, 5186–5195.
24 T. V. Duncan, K. Susumu, L. E. Sinks and M. J. Therien, *J. Am. Chem. Soc.*, 2006, **128**, 9000–9001.
25 N. Aratani, D. Kim and A. Osuka, *Acc. Chem. Res.*, 2009, **42**, 1922–1934.
26 D. Kim, *Multiporphyrin Arrays: Fundamentals and Applications*, Pan Stanford Publishing, 2012.
27 A. Ferri, G. Polzonetti, S. Licoccia, R. Paolesse, D. Favretto, P. Traldi and M. V. Russo, *J. Chem. Soc., Dalton Trans.*, 1998, 4063–4069.
28 S. Richeter, C. Jeandon, J.-P. Gisselbrecht, R. Ruppert and H. J. Callot, *J. Am. Chem. Soc.*, 2002, **124**, 6168–6179.
29 L. Yu, K. Muthukumaran, I. V. Sazanovich, C. Kirmaier, E. Hindin, J. R. Diers, P. D. Boyle, D. F. Bocian, D. Holten and J. S. Lindsey, *Inorg. Chem.*, 2003, **42**, 6629–6647.
30 R. D. Hartnell and D. P. Arnold, *Organometallics*, 2004, **23**, 391–399.
31 Y.-J. Chen, S.-S. Chen, S.-S. Lo, T.-H. Huang, C.-C. Wu, G.-H. Lee, S.-M. Peng and C.-Y. Yeh, *Chem. Commun.*, 2006, 1015–1017.
32 D. Bellows, S. M. Aly, C. P. Gros, M. El Ojaimi, J.-M. Barbe, R. Guilard and P. D. Harvey, *Inorg. Chem.*, 2009, **48**, 7613–7629.
33 P. J. Chmielewski, B. Durlej, M. Siczek and L. Szterenberg, *Angew. Chem., Int. Ed.*, 2009, **48**, 8736–8739.
34 Y. Matano, K. Matsumoto, H. Hayashi, Y. Nakao, T. Kumpulainen, V. Chukharev, N. V. Tkachenko, H. Lemmetyinen, S. Shimizu, N. Kobayashi, D. Sakamaki, A. Ito, K. Tanaka and H. Imahori, *J. Am. Chem. Soc.*, 2012, **134**, 1825–1839.
35 M. Abdelhameed, P.-L. Karsenti, A. Langlois, J.-F. Lefebvre, S. Richeter, R. Ruppert and P. D. Harvey, *Chem. – Eur. J.*, 2014, **20**, 12988–13001.
36 M. Abdelhameed, A. Langlois, P.-L. Karsenti, S. Richeter, R. Ruppert and P. D. Harvey, *Chem. Commun.*, 2014, **50**, 14609–14612.
37 J. Haumesser, J.-P. Gisselbrecht, L. Karmazin-Brelot, C. Bailly, J. Weiss and R. Ruppert, *Organometallics*, 2014, **33**, 4923–4930.
38 H.-W. Jiang, T. Tanaka and A. Osuka, *Chem. Sci.*, 2015, **6**, 6102–6105.
39 N. Fukui, H.-W. Jiang and A. Osuka, *Org. Chem. Front.*, 2017, **4**, 767–772.
40 U. Mitschke and P. Bauerle, *J. Mater. Chem.*, 2000, **10**, 1471–1507.
41 J. L. Segura, *Acta Polym.*, 1998, **49**, 319–344.
42 G. R. Whittell and I. Manners, *Adv. Mater.*, 2007, **19**, 3439–3468.
43 E. Holder, B. M. W. Langeveld and U. S. Schubert, *Adv. Mater.*, 2005, **17**, 1109–1121.
44 G. R. Whittell, M. D. Hager, U. S. Schubert and I. Manners, *Nat. Mater.*, 2011, **10**, 176–188.
45 W.-Y. Wong and C.-L. Ho, *Acc. Chem. Res.*, 2010, **43**, 1246–1256.
46 M. K. Brennaman, R. J. Dillon, L. Alibabaei, M. K. Gish, C. J. Dares, D. L. Ashford, R. L. House, G. J. Meyer, J. M. Papanikolas and T. J. Meyer, *J. Am. Chem. Soc.*, 2016, **138**, 13085–13102.
47 K. A. Green, M. P. Cifuentes, M. Samoc and M. G. Humphrey, *Coord. Chem. Rev.*, 2011, **255**, 2530–2541.
48 J. Rawson, P. J. Angiolillo, P. R. Frail, I. Goodenough and M. J. Therien, *J. Phys. Chem. B*, 2015, **119**, 7681–7689.
49 R. Wang, A. M. Brugh, J. Rawson, M. J. Therien and M. D. E. Forbes, *J. Am. Chem. Soc.*, 2017, **139**, 9759–9762.
50 M.-C. Dul, E. Pardo, R. Lescouëzec, Y. Journaux, J. Ferrando-Soria, R. Ruiz-García, J. Cano, M. Julve, F. Lloret, D. Cangussu, C. L. M. Pereira, H. O. Stumpf, J. Pasán and C. Ruiz-Pérez, *Coord. Chem. Rev.*, 2010, **254**, 2281–2296.
51 M. Bonamico and G. Dessy, *Chem. Commun.*, 1968, 483–484.
52 M. Bonamico, G. Dessy, V. Fares and L. Scaramuzza, *J. Chem. Soc., Dalton Trans.*, 1975, 2250–2256.
53 C. Furlani and M. L. Luciani, *Inorg. Chem.*, 1968, **7**, 1586–1592.
54 R. Shediac, M. H. B. Gray, H. T. Uyeda, R. C. Johnson, J. T. Hupp, P. J. Angiolillo and M. J. Therien, *J. Am. Chem. Soc.*, 2000, **122**, 7017–7033.
55 T. V. Duncan, P. R. Frail, I. R. Miloradovic and M. J. Therien, *J. Phys. Chem. B*, 2010, **114**, 14696–14702.
56 S. M. LeCours, S. G. DiMagno and M. J. Therien, *J. Am. Chem. Soc.*, 1996, **118**, 11854–11864.
57 S. M. LeCours, H.-W. Guan, S. G. DiMagno, C. H. Wang and M. J. Therien, *J. Am. Chem. Soc.*, 1996, **118**, 1497–1503.
58 S. M. LeCours, C. M. Philips, J. C. de Paula and M. J. Therien, *J. Am. Chem. Soc.*, 1997, **119**, 12578–12589.
59 T.-H. Park and M. J. Therien, *Org. Lett.*, 2007, **9**, 2779–2782.
60 K. Susumu and M. J. Therien, *J. Am. Chem. Soc.*, 2002, **124**, 8550–8552.
61 T.-H. Park, *PhD Dissertation*, University of Pennsylvania, 2008.
62 in *CRC, Handbook of Chemistry and Physics*, ed. W. M. Haynes, CRC Press/Taylor and Francis, Boca Raton, FL, 93rd edn., 2012-2013, pp. 8–127.

63 J. Rodriguez, C. Kirmaier and D. Holten, *J. Am. Chem. Soc.*, 1989, **111**, 6500–6506.
64 A. Nakano, Y. Yasuda, T. Yamazaki, S. Akimoto, I. Yamazaki, H. Miyasaka, A. Itaya, M. Murakami and A. Osuka, *J. Phys. Chem. A*, 2001, **105**, 4822–4833.
65 R. Kumble, S. Palese, V. S.-Y. Lin, M. J. Therien and R. M. Hochstrasser, *J. Am. Chem. Soc.*, 1998, **120**, 11489–11498.
66 T. V. Duncan, I. V. Rubtsov, H. T. Uyeda and M. J. Therien, *J. Am. Chem. Soc.*, 2004, **126**, 9474–9475.
67 T. V. Duncan, T. Ishizuka and M. J. Therien, *J. Am. Chem. Soc.*, 2007, **129**, 9691–9703.
68 T. V. Duncan, S. P. Wu and M. J. Therien, *J. Am. Chem. Soc.*, 2006, **128**, 10423–10435.
69 H. A. Frank, J. A. Bautista, J. Josue, Z. Pendon, R. G. Hiller, F. P. Sharples, D. Gosztola and M. R. Wasielewski, *J. Phys. Chem. B*, 2000, **104**, 4569–4577.
70 D. Zigmantas, T. Polívka, R. G. Hiller, A. Yartsev and V. Sundström, *J. Phys. Chem. A*, 2001, **105**, 10296–10306.
71 D. Zigmantas, R. G. Hiller, V. Sundström and T. Polívka, *Proc. Natl. Acad. Sci. U. S. A.*, 2002, **99**, 16760–16765.
72 P. Plaza, D. Laage, M. M. Martin, V. Alain, M. Blanchard-Desce, W. H. Thompson and J. T. Hynes, *J. Phys. Chem. A*, 2000, **104**, 2396–2401.
73 G. E. O'Keefe, G. J. Denton, E. J. Harvey, R. T. Phillips, R. H. Friend and H. L. Anderson, *J. Chem. Phys.*, 1996, **104**, 805–811.
74 J. Koo, J. Park, A. Tronin, R. Zhang, V. Krishnan, J. Strzalka, I. Kuzmenko, H. C. Fry, M. J. Therien and J. K. Blasie, *Langmuir*, 2012, **28**, 3227–3238.
75 J. Park, P. Deria and M. J. Therien, *J. Am. Chem. Soc.*, 2011, **133**, 17156–17159.
76 A. Nayak, J. Park, K. De Mey, X. Hu, T. V. Duncan, D. N. Beratan, K. Clays and M. J. Therien, *ACS Cent. Sci.*, 2016, **2**, 954–966.
77 A. Jouyban and S. Soltanpour, *J. Chem. Eng. Data*, 2010, **55**, 2951–2963.

